HOKKAIDO UNIVERSITY

Title	Photodynamic inactivation of oral bacteria with silver nanoclusters/rose bengal nanocomposite
Author(s)	Shitomi, Kanako; Miyaji, Hirofumi; Miyata, Saori; Sugaya, Tsutomu; Ushijima, Natsumi; Akasaka, Tsukasa; Kawasaki, Hideya
Citation	Photodiagnosis and Photodynamic Therapy, 30, 101647 https://doi.org/10.1016/j.pdpdt.2019.101647
Issue Date	2020-06
Doc URL	http://hdl.handle.net/2115/81582
Rights	©2020. This manuscript version is made available under the CC-BY-NC-ND 4.0 license https://creativecommons.org/licenses/by-nc-nd/4.0/
Rights(URL)	https://creativecommons.org/licenses/by-nc-nd/4.0/
Type	article (author version)
File Information	2020 Shitomi Photodiagnosis Photodyn Ther.pdf

Instructions for use

Hokkaido University Collection of Scholarly and Academic Papers : HUSCAP

Photodynamic inactivation of oral bacteria with silver nanoclusters/rose bengal nanocomposite

Kanako SHITOMI[1], Hirofumi MIYAJI[1]*, Saori MIYATA[1], Tsutomu SUGAYA[1], Natsumi USHIJIMA[2], Tsukasa AKASAKA[3], Hideya KAWASAKI[4]*

[1] Department of Periodontology and Endodontology, Faculty of Dental Medicine, Hokkaido University, N13 W7, Kita-ku, Sapporo 060-8586, Japan

[2] Support Section for Education and Research, Faculty of Dental Medicine, Hokkaido University, N13 W7, Kita-ku, Sapporo 060-8586, Japan

[3] Department of Biomedical, Dental Materials and Engineering, Faculty of Dental Medicine, Hokkaido University, N13 W7, Kita-ku, Sapporo 060-8586, Japan

[4] Department of Chemistry and Materials Engineering, Faculty of Chemistry, Materials and Bioengineering, Kansai University, 3-3-35 Yamate-cho, Suita-shi, Osaka 564-8689, Japan

***Corresponding authors**

Hirofumi MIYAJI, DDS, PhD

Department of Periodontology and Endodontology

Faculty of Dental Medicine, Hokkaido University

N13 W7, Kita-ku, Sapporo 060-8586, Japan

E-mail: miyaji@den.hokudai.ac.jp

Hideya KAWASAKI, PhD

Department of Chemistry and Materials Engineering

Faculty of Chemistry, Materials and Bioengineering, Kansai University

3-3-35 Yamate-cho, Suita-shi, Osaka 564-8689, Japan

E-mail: hkawa@kansai-u.ac.jp

Key words

Aggregatibacter actinomycetemcomitans, Silver nanoclusters (AgNCs)/rose bengal (RB) nanocomposite, Antibacterial photodynamic therapy, *Porphyromonas gingivalis*, Singlet oxygen, *Streptococcus mutans*

Abstract

Antibacterial photodynamic therapy (a-PDT) is a promising anti-infective technique for generation of singlet oxygen ($^1O_2$) to target dental disease. However, conventional organic photosensitizers have some problems for clinical use in terms of cytotoxicity, quenching of a-PDT activity by self-dimerization, and the lack of long-term antibacterial effect. We herein propose silver nanoclusters/rose bengal nanocomposite (AgNCs/RB) as a novel photosensitizer with two primary antibacterial effects: (1) $^1O_2$ generation by irradiated RB and (2) Ag+ ion release from AgNCs. AgNCs/RB irradiated with white light-emitting diode (LED) for a short irradiation time of 1 min significantly decreased the bacterial turbidity of *Streptococcus mutans*, *Porphyromonas gingivalis* and *Aggregatibacter actinomycetemcomitans* (P<0.05). In SEM, TEM and LIVE/DEAD staining images, photoexcited AgNCs/RB reduced *S. mutans* colonization, destroyed the cell membrane, and increased the number of dead cells. The antibacterial efficiency of photoexcited AgNCs/RB was greater than that of AgNCs or RB alone (P<0.05), suggesting a synergistic effect of $^1O_2$ and Ag+ ions from photoexcited AgNCs/RB. By contrast, photoexcited AgNCs/RB did not affect WST-8 and LDH

activities and morphology of NIH3T3 mammalian cells, indicating low cytotoxicity. Interestingly, the antibacterial activity of AgNCs/RB on *S. mutans* was maintained even after the cessation of LED irradiation, indicating a long-term antibacterial effect due to released Ag^+ ions. The present AgNCs/RB photosensitizers provide effective synergistic antibacterial effects for dental a-PDT via $^1O_2$ and Ag^+ ions coupled with low cytotoxicity.

1. Introduction

Antibacterial photodynamic therapy (a-PDT) can be used to control bacterial load via generation of active oxygen species using a light-irradiated photosensitizer. The application of a-PDT has recently received broad attention as future dental treatment, such as dental caries, periodontitis, peri-implantitis, and endodontic therapy [1-3]. Several organic dye photosensitizers, including rose bengal (RB) [4], indocyanine green [5], toluidine blue [6], and methylene blue [4], have been tried for a-PDT. Compared to antibiotic therapy employed in the dental field, the use of dyes for a-PDT has several advantages regarding drug allergy, antibiotic-resistant bacteria [7], and biofilm destruction [8]. However, conventional photosensitizers have some problems for clinical use. Conventional photosensitizers commonly require a cytotoxic organic solvent for formulation [9]. In addition, because $^1O_2$ generated by photosensitizers has a short half-life of microseconds [10], the antibacterial effect disappears shortly after irradiation ceases. The low photostability of organic dye decreases the antibacterial property [11]. Dye molecules generally self-dimerize in water to reduce $^1O_2$ generation [12]. Furthermore, photodynamic events are biologically restricted by rapid enzymatic reduction of dyes [13]. Antibacterial effects of photosensitizers are likely diminished under in vivo conditions containing body fluid. Indeed, some clinical reports showed

that a-PDT did not improve the parameter of periodontal disease compared with conventional therapy [14, 15]. Hence, dental treatment would require a high dose of conventional photosensitizers to subsequently enhance cytotoxic activity [16]. The creation of a novel photosensitizer is required to solve the problems of biosafety.

Silver (Ag) is known to possess antibacterial properties [17]. Many researchers have attempted to apply synthesized Ag substrates for medical applications [18]. Castillo et al. [19] reported that application of silver diamine fluoride to dental caries modified the tooth substrate via Ag deposition and inhibited bacterial cell attachment and caries progression. In addition, dental implants mixed with Ag substrates could obtain antibacterial effects via Ag^+ ion release from their surfaces [18, 20]. Recently, there has been a growing interest in water-soluble Ag nanoclusters (AgNCs) as antibacterial agents because of their ultrasmall sizes (<2 nm) and high antibacterial activity [21-23]. We speculated that a nanocomposite comprising AgNCs and a conventional photosensitizer releases Ag^+ ions by $^1O_2$ acidizing to exhibit long-term antibacterial effects after irradiation. As a result, the nanocomposite of AgNCs/photosensitizer would provide effective synergistic antibacterial effects via $^1O_2$ generated by the photosensitizer coupled with Ag^+ ions released from AgNCs. However, little has been reported on the use of this nanocomposite-based photosensitizer for a-PDT.

In the present study, we for the first time created the nanocomposite of AgNCs and rose bengal (AgNCs/RB) to solve the disadvantages of organic dye photosensitizers and evaluated its antibacterial activity. First, the inhibitory action of AgNCs/RB against oral bacteria *Streptococcus mutans*, *Porphyromonas gingivalis* and *Aggregatibacter actinomycetemcomitans,* was investigated. Then, the cytotoxicity of AgNCs/RB was

assessed using mammalian fibroblastic NIH3T3 cells. We propose two integrated antibacterial strategies for dental a-PDT via AgNCs/RB: bacterial cells are damaged under white light-emitting diode (LED) irradiation by (1) $^1O_2$ generated by photoexcited RB and (2) Ag^+ ions released by AgNCs oxidized by $^1O_2$ (Scheme 1).

2. Materials and methods

2.1 Reagents and bacterial strains

All chemicals were used as received without further purification. Glutathione (reduced form, 98% purity), methotrexate (MTX, 98.0% purity), methanol (99.7% purity), D_2O (99.9% purity), and silver nitrate (99.9% purity) were purchased from FUJIFILM Wako Pure Chemical Corporation Ltd. (Osaka, Japan). Sodium borohydride ($NaBH_4$, 99.99% purity) was purchased from Sigma-Aldrich (St. Louis, MO, USA).

Bacterial strains used in this study were *S. mutans* ATCC 35668, *A. actinomycetemcomitans* ATCC 29522, and *P. gingivalis* ATCC 33277. These strains were kept frozen until analysis. Bacterial stocks were anaerobically and statically incubated in brain heart infusion (BHI) broth (Pearlcore®, Eiken Chemical, Co., Ltd., Tokyo, Japan) supplemented with 0.1% antibiotics (gramicidin D and bacitracin, FUJIFILM Wako Pure Chemical Corporation Ltd.) and 1% sucrose (FUJIFILM Wako Pure Chemical Corporation Ltd.) for *S. mutans*; 1% yeast extract (FUJIFILM Wako Pure Chemical Corporation Ltd.) for *A. actinomycetemcomitans*; and 0.5% yeast extract, 0.0005% hemin, and 0.0001% menadione for *P. gingivalis*. Anaerobic incubation was carried out in an AnaeroPack system using anaerobic jars (Mitsubishi Gas Chemical Company, Inc., Tokyo, Japan).

2.2.1 Synthesis of AgNCs/RB

AgNCs [i.e., $Ag_{32}(SG)_{19}$] were obtained by ultraviolet (UV) photomediated size-focusing synthesis as previously described [24]. This photomediated size-focusing synthesis comprises a two-step protocol: (i) the reduction of Ag ions by $NaBH_4$ to form polydisperse AgNC intermediates and (ii) the subsequent photomediated size-focusing of these intermediates under 365 nm UV irradiation to produce monodisperse $Ag_{32}(SG)_{19}$. Finally, $Ag_{32}(SG)_{18}$ was vacuum dried and kept at 4°C until further use.

AgNCs/RB was prepared through the interaction between AgNCs and RB. A 1 mM RB solution and 1 mM AgNCs solution were prepared as stock solutions. The RB solution was mixed with the AgNCs solution in mole ratio of 1:0.3 (AgNCs:RB). The resultant solution was stirred at 200 rpm for 2 h using a magnetic stirrer. Thereafter, the solution was purified with a centrifugal ultrafiltration tube (Amicon® Ultra-Centrifugal Filters, 3 KD, Merck, Darmstadt, Germany) to discard free RB. After centrifugal ultrafiltration, the filtrate solution did not contain RB, indicating the binding of RB into the AgNCs in the nanocomposite with mole ratio of 1:0.3 (AgNCs:RB).

2.2.2 Characterization of AgNCs/RB

UV-vis (absorption) spectra were recorded using a UV-vis-NIR spectrophotometer (V-670, JASCO, Tokyo, Japan) and a fluorometer (FP-6300, JASCO, Tokyo, Japan). Zeta potential measurements were performed on a Malvern Zetasizer Nano ZS instrument (Malvern Instruments Ltd., Worcestershire, UK) equipped with a HeNe laser operating at 632.8 nm. Inductively coupled plasma mass spectrometry (ICP-MS) measurements were carried out with a quadrupole ICP-MS instrument (7900 ICP-MS, Agilent Technologies, Santa Clara, CA, USA). The linear calibration curve

was set up between 1 and 1000 ng/L Ag (I) in either HAc 3% (v/v) or EtOH 50% (v/v) and was recorded.

2.2.3 Detection of $^1O_2$ generation by AgNCs/RB

$^1O_2$ generated by photoexcited AgNCs/RB under white LED light irradiation (wavelength of 420–750 nm, 80 mW/cm^2, SPF-D2, Shodensha, Osaka, Japan) was evaluated using MTX as a chemical probe of $^1O_2$. MTX can selectively react with $^1O_2$, resulting in increased fluorescence intensity [25]. The concentration of the AgNCs was adjusted to be equal absorbance (ca. 0.1) at 532 nm. A 10 mM stock solution of MTX in *N,N*-dimethylformamide was prepared and then added to a 2-mL aqueous solution (D_2O) to yield a final concentration of 20 μM MTX. The solutions were then irradiated with a white LED light. Fluorescence spectra were recorded using a spectrofluorometer.

2.2.4 Release of silver by AgNCs/RB

The aqueous solution of AgNCs/RB (absorbance of 0.4 at 490 nm) was irradiated by white light LED. The resultant solution of AgNCs/RB was separated with a centrifugal ultrafiltration tube (Amicon® Ultra-Centrifugal Filters, 3 KD, Merck). After centrifugal ultrafiltration, the filtrate solution did not contain AgNCs/RB but contained silver released from AgNCs/RB after LED irradiation. The amount of silver in the filtrate solution was evaluated by ICP-MS.

2.3 Antibacterial effects of AgNCs/RB

AgNCs/RB [final concentration: 0 (absence), 0.01, 0.1, 1, and 10 μg/mL] was dissolved in a suspension containing *S. mutans* [final concentration: 5.5×10^6

colony-forming unit (CFU)/mL], *A. actinomycetemcomitans* (final concentration: 1.1×10^6 CFU/mL) or *P. gingivalis* (final concentration: 3.7×10^7 CFU/mL) taken at log growth phase. After white LED light irradiation for 1 min at a distance of 2 cm, the suspension was incubated for 24 h under anaerobic incubation at 37°C. Thereafter, the turbidity of each suspension was measured using a colorimeter (CO7500 Colourwave, Funakoshi Co. Ltd., Tokyo, Japan) at an absorbance of 590 nm.

To observe the morphology of *S. mutans,* the suspension containing *S. mutans* and AgNCs/RB [final concentration: 0 (absence) and 10 μg/mL] was irradiated by white LED light for 1 min at a distance of 2 cm and incubated for 24 h. The samples were fixed in 2.5% glutaraldehyde in 0.1 M sodium cacodylate buffer (pH 7.4) and dehydrated in ethanol for scanning electron microscopy (SEM; S-4000, Hitachi Ltd., Tokyo, Japan) at an accelerating voltage of 10 kV after Pt-Pd coating. Fixed samples were postfixed in 1% OsO_4 and 0.1 M sodium cacodylate buffer (pH 7.4) at 4°C for 1 h. Subsequently, samples were dehydrated in ethanol, infiltrated with propylene oxide, embedded in Epon, and characterized after slicing using transmission electron microscopy (TEM; JEM-1400, JEOL Ltd., Tokyo, Japan) at 200 kV acceleration voltage. In addition, some samples were stained by the LIVE/DEAD BacLight Bacterial Viability Kit (Thermo Fisher Scientific, Waltham, MA, USA) and observed using fluorescence microscopy equipped with a 20× objective lens (BZ-9000 BioRevo, Keyence Corporation, Osaka, Japan).

To compare the antibacterial effect of the nanocomposite and its constituents, AgNCs (10 μg/mL), AgNCs/RB (10.35 μg/mL), or RB (0.35 μg/mL) was added to a suspension containing *S. mutans* (final concentration: 5.5×10^6 CFU/mL) or *A. actinomycetemcomitans* (final concentration: 1.1×10^6 CFU/mL) and white LED light

irradiated for 0 or 1 min at a distance of 2 cm. We used $Ag_{32}(SG)_{19}$ NCs with the molecular weight of 9273 g/mol, while that of RB is 974 g/mol. The RB solution was mixed with the AgNCs solution in mole ratio of 1:0.3 (AgNCs:RB), corresponding to the concentration of AgNCs (10 μg/mL) and RB (0.35 μg/mL), respectively.

After 24-h culture, the turbidity of each suspension was measured. In addition, *S. mutans* suspensions containing AgNCs/RB (1 μg/mL) were irradiated for 0, 30, 60, 90, or 120 s to assess the time-dependent effect of a-PDT. After incubation for 24 h, the turbidity was measured. To investigate the influence of Ag^+ ion release on antibacterial activity, BHI medium containing 10 μg/mL AgNCs/RB was photoexcited with LED irradiation for 1 min at a distance of 2 cm. At 10, 60, and 900 s after irradiation, the *S. mutans* suspension was mixed into the medium. The turbidity of the 24-h cultured suspension was then measured.

2.4 Cytotoxic evaluation of AgNCs/RB

To compare the cytotoxicity of the nanocomposite, AgNCs/RB (0 and 10 μg/mL) was added to a suspension containing 1×10^4 mouse osteoblastic NIH3T3 cells (RIKEN BioResource Research Center, Tsukuba, Japan) and irradiated with white LED light for 0 or 1 min at a distance of 2 cm. Cell culture was performed in 96-well plates using culture medium (minimum essential medium alpha, GlutaMAX-I, Thermo Fisher Scientific) supplemented with 10% fetal bovine serum (Qualified FBS, Thermo Fisher Scientific) and 1% antibiotics (penicillin-streptomycin, Thermo Fisher Scientific) at 37°C with 5% CO_2. Cytotoxicity after 24-h incubation was determined using the water-soluble tetrazolium salt (WST)-8 assay (Cell Counting Kit-8, Dojindo Laboratories, Mashiki, Japan) and lactate dehydrogenase (LDH) assay (Cytotoxicity

LDH Assay Kit-WST, Dojindo Laboratories). The absorbance at 450 nm (WST-8) or 490 nm (LDH) was measured on a microplate reader (ETY-300, Toyo Sokki, Yokohama, Japan).

In addition, vinculin/F-actin double staining of incubated cells was performed. Cells cultured on glass-based dishes (AGC Techno Glass Co. Ltd., Haibara, Japan) were fixed in 3.5% paraformaldehyde for 5 min, permeabilized with 0.5% Triton X-100 in phosphate-buffered solution (PBS, FUJIFILM Wako Pure Chemical Corporation Ltd.) for 10 min and then blocked with 1% bovine serum albumin (BSA) [7.5 w/v% Albumin Dulbecco's-PBS(-) Solution, from Bovine Serum, FUJIFILM Wako Pure Chemical Corporation Ltd.]/PBS for 30 min. A staining solution was prepared by mixing 4.0 μg/mL anti-vinculin monoclonal antibody (Anti-Vinculin Alexa Fluor 488, eBioscience, San Diego, CA, USA), 0.12 μg/mL phalloidin (Acti-stain 555 fluorescent Phalloidin, Cytoskeleton Inc., Denver, CO, USA) dissolved in methanol, and 6.0 μg/mL 4',6-diamidino-2-phenylindole solution (Dojindo Laboratories) in BSA. The mixture was kept shaking for 1 h at 37°C. After 24-h incubation at 4°C, the sample was washed and observed using fluorescence microscopy equipped with a 20× objective lens. Some samples were stained using the LIVE/DEAD Viability/Cytotoxicity Kit for mammalian cells (Thermo Fisher Scientific) and observed using fluorescence microscopy.

2.5 Statistical analysis

Statistical analyses were performed using Scheffé and Games-Howell tests. *P* values <0.05 were considered statistically significant. All statistical procedures were performed using software package SPSS 11.0 (IBM Corporation, Armonk, NY, USA).

3. Results

3.1 Synthesis and characterization of AgNCs/RB

Fig. 1A shows the UV-vis spectra of AgNCs, RB, and AgNCs/RB. The AgNCs showed an absorption peak at 485 nm, which is consistent with that of $Ag_{32}(SG)_{19}$ [24]. Upon conjugation of RB with the AgNCs, both AgNC and RB absorptions were observed at around 500 and 550 nm in AgNCs/RB, respectively. This indicates the binding of RB into the AgNCs in the nanocomposite. The binding was also supported by the decrease in the ξ value from −27 mV (AgNCs) to −51 mV (AgNCs/RB) due to the negatively charged RB (Fig. 1B).

3.2 Detection of $^1O_2$ generation and silver release by photoexcited AgNCs/RB

$^1O_2$ generation by photoexcited AgNCs/RB was evaluated using a chemical trap $^1O_2$ probe, MTX. AgNCs/RB has broad absorbance in the UV-vis range of <700 nm. Hence, a white LED with wavelength of 400–700 nm was chosen as an effective photoexcitation source for the nanocomposite. Fluorescence spectra of MTX in the presence of AgNCs/RB in D_2O were obtained. There was no change in fluorescence spectra of MTX in the dark. However, under white LED irradiation for 10 min, fluorescence intensities at 466 nm increased over time due to the oxidation of MTX by $^1O_2$ generated by the nanocomposite (Fig. 1C) [26].

Fig. 1D shows the UV-vis spectra of AgNCs/RB before and after white LED irradiation for 20 min. It is clear from the absorbance decrease that LED irradiation caused the degradation of both RB and the AgNCs in the nanocomposite: the absorbance decreased at 550 nm for RB and at 440 nm for AgNCs. The absorption decrement of AgNCs after LED irradiation was larger in AgNCs/RB (~5%) than that of

AgNCs alone (~1%) (Fig. 1E). This suggests the enhanced photoinduced degradation of AgNCs in the conjugate. The amount of Ag^+ ion released from the aqueous solution (absorbance of 0.4 at 490 nm) of AgNCs/RB during LED irradiation for 20 min was evaluated by ICP-MS. This evaluation revealed that 370 ppb Ag was released, corresponding to 0.34% Ag release from the nanocomposite. The released amount is very low, but it is a sufficiently high concentration to show antibacterial activity [22].

3.3 Antibacterial effects of photoexcited AgNCs/RB

The turbidities of oral bacterial suspensions are shown in Fig. 2. Application of AgNCs/RB and white LED irradiation dose-dependently inhibited the growth of *S. mutans*, *P. gingivalis*, and *A. actinomycetemcomitans* (P<0.05). Especially, 10 μg/mL of AgNCs/RB exhibited a significant growth inhibitory effect compared to control (no application). SEM images of *S. mutans* at 24 h after incubation are shown in Fig. 2B. In control (no application of AgNCs/RB), marked colonization of *S. mutans* was observed on the culture dish. In contrast, the sample that received AgNCs/RB (10 μg/mL) and white LED treatment showed slight bacterial cell accumulation. In TEM images, *S. mutans* cells of control displayed a spherical cell body enclosed by an intact cell membrane. In contrast, the cell body frequently exhibited an irregular shape with destruction of the cell membrane in the AgNCs/RB and LED applied group (Fig. 2B). In the assessment of LIVE/DEAD BacLight staining, *S. mutans* in control (no application of AgNCs/RB) was mostly stained in green, indicating live cells. When AgNCs/RB (10 μg/mL) and white LED were applied, *S. mutans* frequently stained red, indicating dead cells (Fig. 2B).

To compare the antibacterial activities of AgNCs/RB, AgNCs, and RB, the amounts of AgNCs and RB were adjusted to employ in culture test (mole ratio of 1:0.3 AgNCs:RB). Fig. 3A and B show the turbidity of *S. mutans* and *A. actinomycetemcomitans*, respectively. When white LED irradiation was not applied, the turbidities of *S. mutans* and *A. actinomycetemcomitans* were comparable in all groups. However, white LED irradiation with the application of AgNCs/RB or RB significantly decreased the turbidity of bacterial cells when compared to control (no application of AgNCs/RB) (P<0.05). The combination of AgNCs/RB with white LED irradiation significantly inhibited the turbidity increase compared to AgNCs or RB (P<0.05). The application of LED irradiation to AgNCs/RB time-dependently decreased the turbidity of *S. mutans* (Fig. 3C). To assess the antibacterial effect of released Ag^+ ions, the bacterial suspension was mixed into BHI medium containing 10 μg/mL AgNCs/RB at 10, 60, and 900 s after white LED irradiation. A short wait time (10 s) suppressed the turbidity of *S. mutans*, suggesting that Ag^+ ions released by oxidation of AgNCs exerted the antibacterial activity (Fig. 3D). However, long wait times (60 and 900 s) did not reduce the turbidity of *S. mutans*.

3.4 Cytotoxic effects of photoexcited AgNCs/RB

The results of WST-8 and LDH and activity assays are presented in Fig. 4A. WST-8 and LDH activities of fibroblastic cells were comparable in all groups after incubation for 24 h. The LIVE/DEAD BacLight assay showed that cultured cells exhibited green fluorescence (live cells) in control (no application of AgNCs/RB) and AgNCs/RB applied groups (Fig. 4B). In addition, positive staining for vinculin and

F-actin, which are associated with cell adhesion and spreading, was detected, regardless of the application of AgNCs/RB and white LED irradiation (Fig. 4B).

4. Discussion

In the present study, the combination of AgNCs/RB with white LED irradiation significantly suppressed the growth of oral bacteria. These results were supported by TEM observation and LIVE/DEAD staining because photoexcited AgNCs/RB killed bacterial cells. As the result of fluorescence intensity measurement using MTX, photoexcited AgNCs/RB time-dependently generated $^1O_2$. Therefore, the antibacterial effects of AgNCs/RB were mainly conducted by RB via $^1O_2$ generation. Oxidative stress by reactive oxygen species (ROS), such as $^1O_2$, superoxide, hydroxyl radicals, and hydrogen peroxide, may attack unsaturated fatty acids in the membrane and stimulate lipid peroxidation to form toxic substances such as aldehydes [27]. In addition, ROS interrupts DNA replication [28] and promotes amino acid degradation in protein [29]. Furthermore, the application of AgNCs/RB and LED irradiation diminished the turbidity of periodontal pathogen bacteria *A. actinomycetemcomitans* and *P. gingivalis*, suggesting an antibacterial effect of photoexcited AgNCs/RB on periodontal bacteria. Since $^1O_2$ is effective against Gram-negative and -positive bacteria [30], a-PDT using AgNCs/RB may be beneficial as a broad-spectrum treatment against various dental conditions. However, in dental therapy, destruction of the bacterial biofilm is the primary target of inflammatory disease treatment. In contrast to antibiotic therapy, some reports showed that a-PDT destroys bacterial cells in the biofilm [31, 32]. Hence, AgNCs/RB must be evaluated in biofilm models before its use as a-PDT can be fully realized.

Previously, we reported that AgNCs undergo light-induced degradation [24]. The present results suggest that light-induced degradation of AgNCs is more enhanced in the conjugate of AgNCs with RB from the absorbance decrease of AgNCs (Fig. 1E). We hypothesized that the AgNCs conjugated to RB are oxidized by $^1O_2$ from RB under light irradiation, resulting in Ag^+ ion release. The amount of released Ag confirmed by ICP-MS is sufficient to yield antibacterial activity. Because the activity of $^1O_2$ immediately disappeared after conversion into $^3O_2$ in less than a few microseconds [33], it was considered that the antibacterial effect of $^1O_2$ was soon reduced after the cessation of LED irradiation. However, we found that photoexcited AgNCs/RB suppressed *S. mutans* growth even after a waiting period (10 s; Fig. 3D). Therefore, we speculate that released Ag^+ ions remain in the BHI medium for a longer time than $^1O_2$ to continuously exert the antibacterial activity of AgNCs/RB. Thus, AgNCs/RB as a-PDT likely has dual antibacterial effects via $^1O_2$ generation by RB and Ag^+ ion release from AgNCs. A previous report revealed that Ag^+ ions penetrate the cell body to inhibit DNA replication and inactivate protein [34]. We also found the antibacterial activity disappeared after a waiting period of 60 and 900 s. The released Ag^+ ions may form compounds with other substances in the BHI medium due to its low ionization tendency. For instance, Ostermeyer et al. [35] reported that BSA, as a model protein, could absorb Ag^+ ions released from Ag nanoparticles to form a chelate complex.

In general, antibacterial materials frequently show cytotoxic adverse effects [34]. In the present study, cell morphology and WST-8 and LDH activities of NIH3T3 mammalian cells were comparable in all groups, regardless of LED irradiation. Hence, this study revealed AgNCs/RB possesses low cytotoxic effects in fibroblastic cells. From the results of zeta potential measurements, AgNCs/RB was more negatively

charged than AgNCs, suggesting that the stability of AgNCs/RB dispersion would be improved to enhance the biosafety. The dispersion degree of a nanomaterial plays an important role in biocompatibility. Guo et al. [36] reported that well-dispersed nanomaterials, or carbon nanotubes, could improve their cytocompatibility in the MTT assay. In addition, a conventional dye, methylene blue, reportedly inhibits cell proliferation at the concentration of clinical use for a-PDT application [16]. The advantages of AgNCs/RB include high cytocompatibility as well as great antibacterial effects via $^1O_2$ generation and Ag^+ ion release in comparison with conventional photosensitizers.

5. Conclusion

We created AgNCs/RB as a novel photosensitizer with dual antibacterial action for dental a-PDT: photoexcited AgNCs/RB could generate both $^1O_2$ and Ag^+ ions to exhibit synergistic bactericidal effects. AgNCs/RB irradiated by white LED dose- and time-dependently reduced the turbidity of oral bacteria *S. mutans*, *A. actinomycetemcomitans*, and *P. gingivalis.* Photoexcited AgNCs/RB was effective even at 10 s after LED irradiation ceased. Furthermore, the application of AgNCs/RB showed low cytotoxicity against fibroblastic NIH3T3 cells. Therefore, AgNCs/RB and white LED is likely beneficial as new material for a-PDT.

Conflicts of interest

The authors have no conflict of interest to declare.

Acknowledgements

The authors acknowledge Dr. Ayumi Saeki (Department of Oral Pathobiological Science, Hokkaido University Faculty of Dental Medicine) for her technical assistance in the assessments of antibacterial effects of AgNCs/RB. This work was supported by JSPS KAKENHI (Grant Nos. JP15H03520 and JP16K11822) and the Tanaka Kikinzoku Memorial Foundation. The authors declare no potential conflicts of interest with respect to the authorship and/or publication of this article.

References

[1] M. Wilson, Lethal photosensitization of oral bacteria and its potential application in the photodynamic therapy of oral infections, Photochem Photobiol Sci. 3 (5) (2004) 412-418, https://doi.org/10.1039/B211266C

[2] S. Rajesh, E. Koshi, K. Philip, A. Mohan, Antimicrobial photodynamic therapy: An overview, J Indian Soc Periodontol. 15 (4) (2011) 323-327, https://doi.org/10.4103/0972-124X.92563

[3] G. Sivaramakrishnan, K. Sridharan, Photodynamic therapy for the treatment of peri-implant diseases: A network meta-analysis of randomized controlled trials, Photodiagnosis Photodyn Ther. 21 (2018) 1-9, https://doi.org/10.1016/j.pdpdt.2017.10.013

[4] P. Soria-Lozano, Y. Gilaberte, M.P. Paz-Cristobal, L. Pérez-Artiaga, V. Lampaya-Pérez, J. Aporta, V. Pérez-Laguna, I. García-Luque, M.J. Revillo, A. Rezusta, In vitro effect photodynamic therapy with differents photosensitizers on cariogenic microorganisms, BMC Microbiol. 15 (2015) 187, https://doi.org/10.1186/s12866-015-0524-3

[5] S. Parker, The use of diffuse laser photonic energy and indocyanine green photosensitiser as an adjunct to periodontal therapy, Br Dent J. 215 (4) (2013) 167-171, https://doi.org/10.1038/sj.bdj.2013.790

[6] L.P. Rosa, F.C. da Silva, S.A. Nader, G.A. Meira, M.S. Viana, Antimicrobial photodynamic inactivation of staphylococcus aureus biofilms in bone specimens using methylene blue, toluidine blue ortho and malachite green: An in vitro study, Arch Oral Biol. 60 (5) (2015) 675-680, https://doi.org/10.1016/j.archoralbio.2015.02.010

[7] N. Fotinos, M. Convert, J.C. Piffaretti, R. Gurny, N. Lange, Effects on gram-negative and gram-positive bacteria mediated by 5-aminolevulinic acid and 5-aminolevulinic acid derivatives, Antimicrob Agents Chemother. 52 (4) (2008) 1366-1373, https://doi.org/10.1128/AAC.01372-07

[8] F. Cieplik, L. Tabenski, W. Buchalla, T. Maisch, Antimicrobial photodynamic therapy for inactivation of biofilms formed by oral key pathogens, Front Microbiol. 5 (2014) 405, https://doi.org/10.3389/fmicb.2014.00405

[9] J. Crooks. Haemolytic jaundice in a neonate after intra-amniotic injection of methylene blue. Arch Dis Child. 57 (11) (1982) 872–873, https://doi.org/10.1136/adc.57.11.872

[10] A.A. Gorman, M.A. Rodgers, New trends in photobiology: Current perspectives of singlet oxygen detection in biological environments, J Photochem Photobiol B. 14 (3) (1992) 159-176, https://doi.org/10.1016/1011-1344(92)85095-C

[11] R. Bonnett, Photosensitizers of the porphyrin and phthalocyanine series for photodynamic therapy, Chem. Soc. Rev. 24 (1) (1995) 19-33, https://doi.org/10.1039/CS9952400019

[12] D.B. Tada, L.L. Vono, E.L. Duarte, R. Itri, P.K. Kiyohara, M.S. Baptista, L.M. Rossi, Methylene blue-containing silica-coated magnetic particles: a potential magnetic carrier for photodynamic therapy, Langmuir, 23 (15) (2007) 8194-8199, https://doi.org/10.1021/la700883y

[13] X. He, X. Wu, K. Wang, B. Shi, L. Hai, Methylene blue-encapsulated phosphonate-terminated silica nanoparticles for simultaneous in vivo imaging and photodynamic therapy, Biomaterials, 30 (2009) 5601–5609, https://doi.org/10.1016/j.biomaterials.2009.06.030

[14] S.H. Bassir, N. Moslemi, R. Jamali, S. Mashmouly, R. Fekrazad, N. Chiniforush, A.R. Shamshiri, H. Nowzari, Photoactivated disinfection using light-emitting diode as an adjunct in the management of chronic periodontitis: a pilot double-blind split-mouth randomized clinical trial, J Clin Periodontol, 40 (1) (2013) 65-72, https://doi.org/10.1111/jcpe.12024

[15] V.H. Luchesi, S.P. Pimentel, M.F. Kolbe, F.V. Ribeiro, R.C. Casarin, F.H. Nociti Jr, E.A. Sallum, M.Z. Casati, Photodynamic therapy in the treatment of class II furcation: a randomized controlled clinical trial, J Clin Periodontol, 40 (8) (2013) 781-788, https://doi.org/10.1111/jcpe.12121

[16] S. Miyata, H. Miyaji, H. Kawasaki, M. Yamamoto, E. Nishida, H. Takita, T. Akasaka, N. Ushijima, T. Iwanaga, T. Sugaya, Antimicrobial photodynamic activity and cytocompatibility of $Au_{25}(Capt)_{18}$ clusters photoexcited by blue LED light irradiation, Int J Nanomedicine. 12 (2017) 2703-2716, https://doi.org/10.2147/IJN.S131602

[17] K. Zheng, M.I. Setyawati, D.T. Leong, J. Xie, Antibacterial Silver Nanomaterials, Coord Chem Rev. 357 (2018) 1-17, https://doi.org/10.1016/j.ccr.2017.11.019

[18] J.M. Corrêa, M. Mori, H.L. Sanches, A.D. da Cruz, E. Poiate Jr., I.A. Poiate, Silver nanoparticles in dental biomaterials, Int J Biomater. 2015 (2015) 485275, https://doi.org/10.1155/2015/485275

[19] J.L. Castillo, S. Rivera, T. Aparicio, R. Lazo, T.C. Aw, L.L. Mancl, P. Milgrom, The short-term effects of diammine silver fluoride on tooth sensitivity: a randomized controlled trial, J Dent Res. 90 (2) (2011) 203-208, https://doi.org/10.1177/0022034510388516

[20] J. Wang, J. Li, G Guo, Q. Wang, J. Tang, Y. Zhao, H. Qin, T. Wahafu, H. Shen, X Liu, X. Zhang, Silvernanoparticles-modified biomaterial surface resistant to staphylococcus: new insight into the antimicrobial action of silver, Sci Rep. 6 (2016) 32699, https://doi.org/10.1038/srep32699

[21] A. Sangsuwan, H. Kawasaki, Y. Matsumura, Y. Iwasaki, Antibacterial silver nanoclusters bearing biocompatible phosphorylcholine-based zwitterionic protection, Bioconjug Chem. 27 (10) (2016) 2527-2533, https://doi.org/10.1021/acs.bioconjchem.6b00455

[22] C. Tominaga, K. Shitomi, H. Miyaji, H. Kawasaki, Antibacterial photocurable acrylic resin coating using a conjugate between silver nanoclusters and alkyl quaternary ammonium, ACS Appl. Nano Mater. 1 (9) (2018) 4809-4818, https://doi.org/10.1021/acsanm.8b01010

[23] K. Shitomi, H. Miyaji, S. Miyata, E. Nishida, K. Mayumi, T. Sugaya, H. Kawasaki, Human dentin coated with silver nanoclusters exhibits antibacterial activity against Streptococcus mutans, Nano Biomed. 11 (1) (2019) 21-28, https://doi.org/10.11344/nano.11.21

[24] C. Tominaga, H. Hasegawa, K. Yamashita, R. Arakawa, H. Kawasaki, UV photo-mediated size-focusing synthesis of silver nanoclusters, RSC Adv. 6 (77) (2016) 73600-73604, https://doi.org/10.1039/C6RA10892J

[25] K. Hirakawa, Fluorometry of singlet oxygen generated via a photosensitized reaction using folic acid and methotrexate, Anal Bioanal Chem. 393 (3) (2009) 999-1005, https://doi.org/10.1007/s00216-008-2522-x

[26] M. Yamamoto, K. Shitomi, S. Miyata, H. Miyaji, H. Aota, H. Kawasaki, Bovine serum albumin-capped gold nanoclusters conjugating with methylene blue for efficient $^1O_2$ generation via energy transfer, J Colloid Interface Sci. 510 (2018) 221-227, https://doi.org/10.1016/j.jcis.2017.09.011

[27] E. Birben, U.M. Sahiner, C. Sackesen, S. Erzurum, O. Kalayci, Oxidative stress and antioxidant defense, World Allergy Organ J. 5 (1) (2012) 9-19, https://doi.org/10.1097/WOX.0b013e3182439613

[28] N.R. Jena, DNA damage by reactive species: Mechanisms, mutation and repair, J Biosci. 37 (3) (2012) 503-517. https://doi.org/10.1007/s12038-012-9218-2.

[29] B.S. Berlett, E.R. Stadtman, Protein oxidation in aging, disease, and oxidative stress, J Biol Chem. 272 (33) (1997) 20313-20316, https://doi.org/10.1074/jbc.272.33.20313

[30] T.A. Dahl, W.R. Midden, P.E. Hartman, Comparison of killing of gram-negative and gram-positive bacteria by pure singlet oxygen, J Bacteriol. 171 (4) (1989) 2188-2194, https://doi.org/10.1128/jb.171.4.2188-2194.1989

[31] I.C. Zanin, R.B. Gonçalves, A.B. Junior, C.K. Hope, J. Pratten, Susceptibility of Streptococcus mutans biofilms to photodynamic therapy: an in vitro study, J Antimicrob Chemother, 56 (2005) 324-330, https://doi.org/10.1093/jac/dki232

[32] S. Wood, D. Metcalf, D. Devine, C. Robinson, Erythrosine is a potential photosensitizer for the photodynamic therapy of oral plaque biofilms. J Antimicrob Chemother, 57 (2006) 680-684, https://doi.org/10.1093/jac/dkl021

[33] J. Moan, K. Berg, The photodegradation of porphyrins in cells can be used to estimate the lifetime of singlet oxygen, Photochem Photobiol. 53 (4) (1991) 549-553, https://doi.org/10.1111/j.1751-1097.1991.tb03669.x

[34] L. Rizzelloa, P.P. Pompa, Nanosilver-based antibacterial drugs and devices: Mechanisms, methodological drawbacks, and guidelines, Chem Soc Rev. 43 (5) (2014) 1501-1518, https://doi.org/10.1039/c3cs60218d

[35] A.K. Ostermeyer, C.K. Mumuper, L. Semprini, T. Radniecki, Influence of bovine serum albumin and alginate on silver nanoparticle dissolution and toxicity to nitrosomonas europaea, Environ Sci Technol. 47 (24) (2013) 14403-14410, https://doi.org/10.1021/es4033106

[36] Y.K. Guo, W. Chen, Q. Xiong, Q.X. Ren, L. Sun, B. Han, X.J. Li, Chemically modified multiwalled carbon nanotubes improve the cytocompatibility, Mater Res Express. 4 (12) (2017) 125801, https://doi.org/10.1088/2053-1591/aa9d21

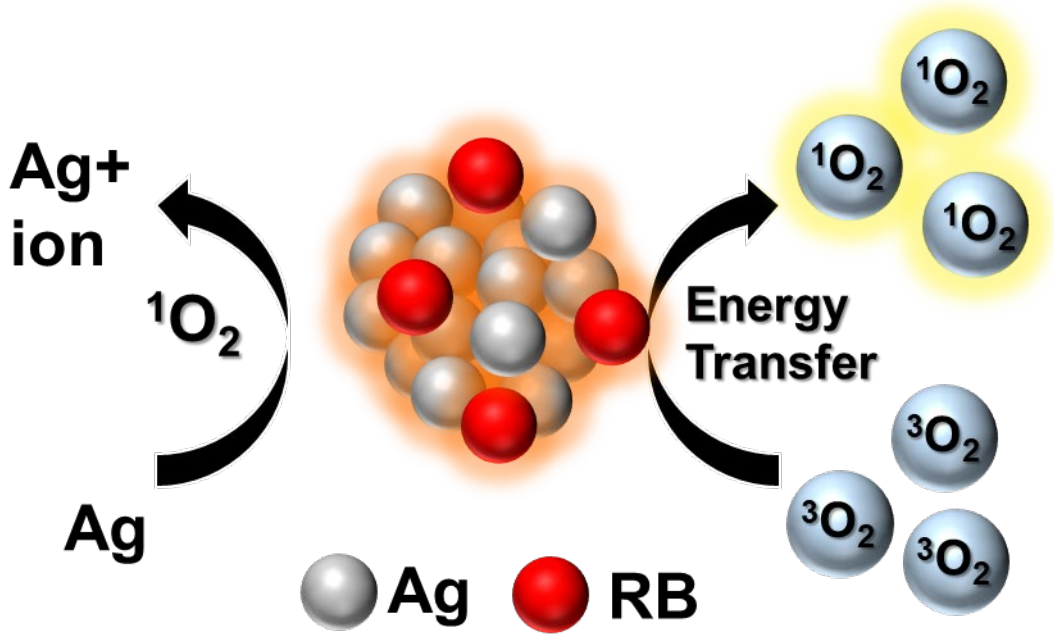

Scheme 1. Silver nanoclusters/rose bengal (AgNCs/RB) nanocomposite-based photosensitizer with dual antibacterial effects ($^1O_2$ and Ag^+ ions)

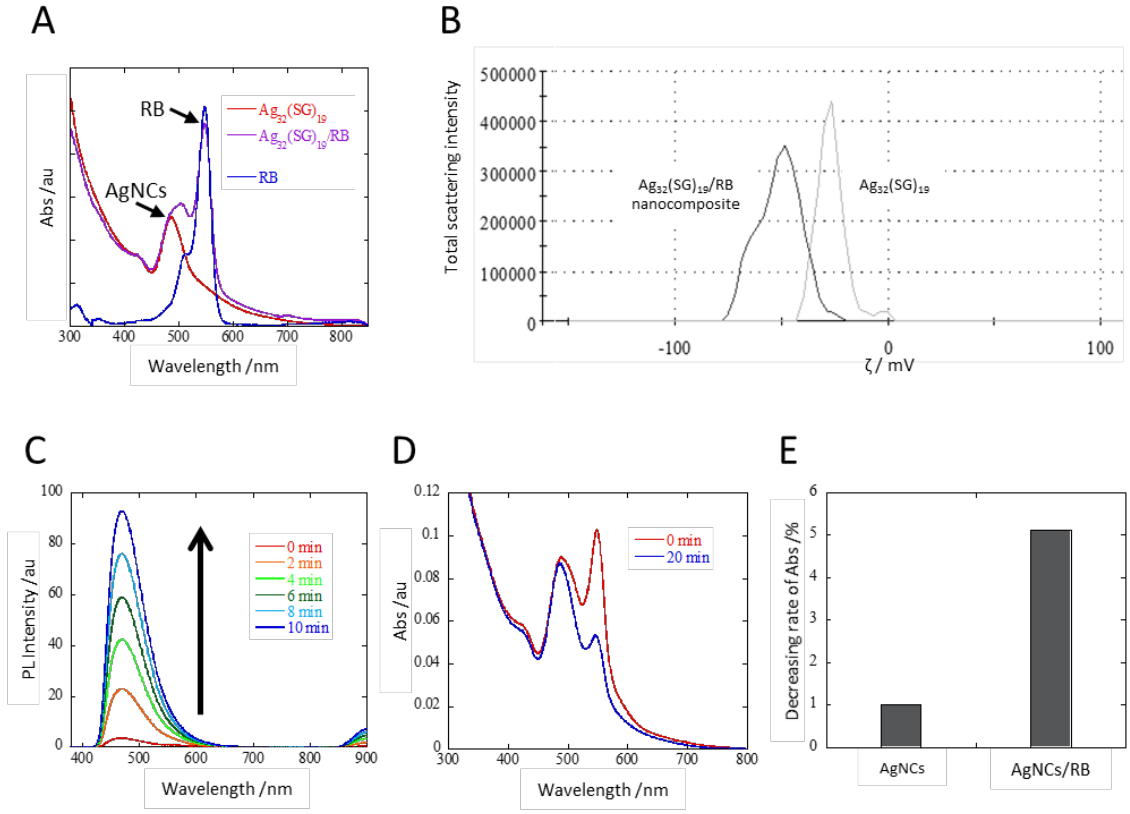

Fig. 1. Characterization of AgNCs/RB

(A) UV-vis spectra of AgNCs (red line), AgNCs/RB (purple line), and RB (blue line). (B) Zeta potentials of AgNCs and AgNCs/RB. (C) Fluorescence spectra of an MTX-containing solution of AgNCs/RB. (D) UV-vis spectra of AgNCs/RB before (red line, 0 min) and after (blue line, 20 min) white LED irradiation. (E) Decreasing ratio of absorbance of AgNCs and AgNCs/RB following white LED irradiation. Abs, absorbance; AgNCs, silver nanoclusters; au, arbitrary unit; LED, light-emitting diode; MTX, methotrexate; PL, photoluminescence; RB, rose bengal; UV, ultraviolet.

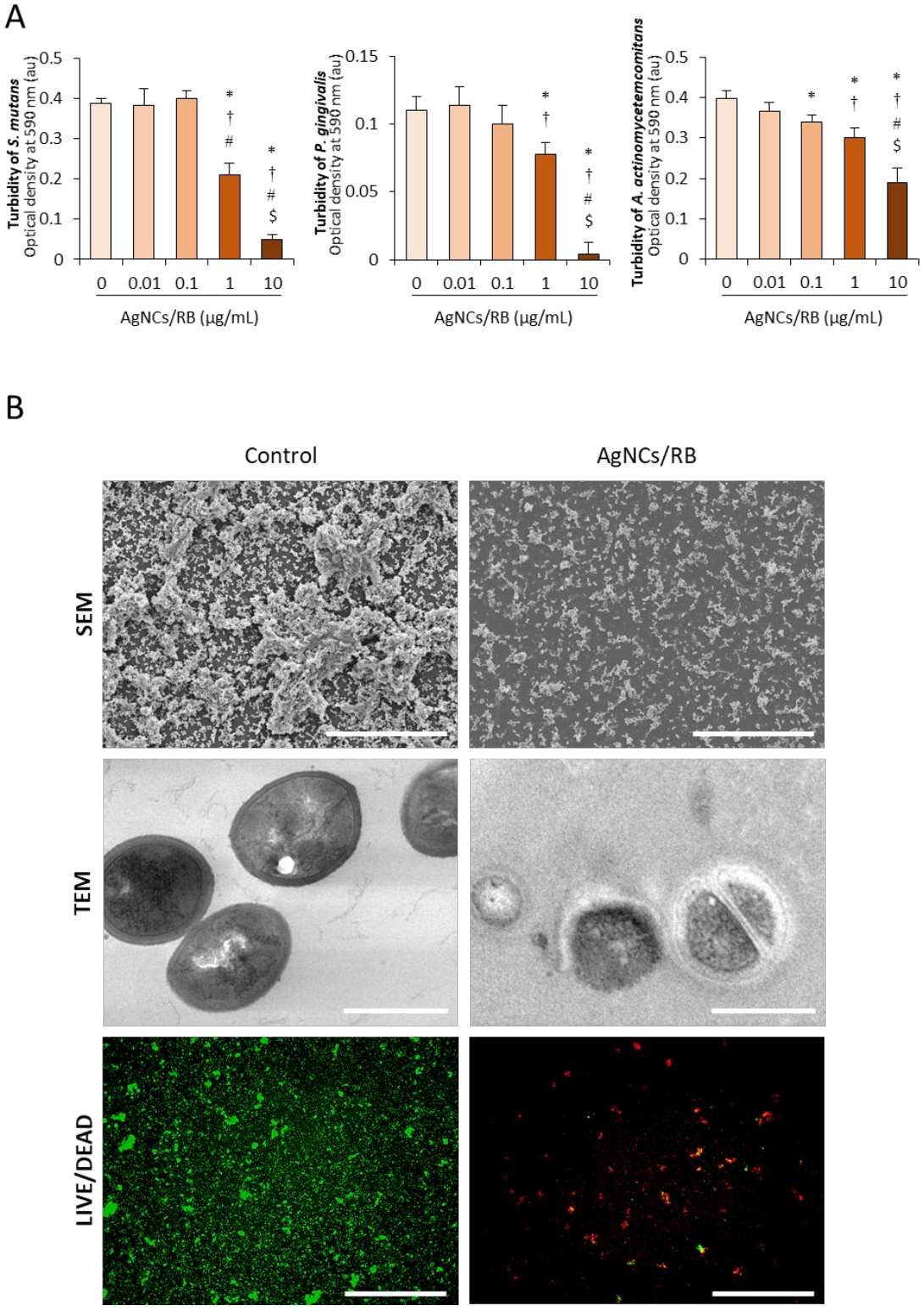

Fig. 2. Evaluation of antibacterial activity of AgNCs/RB

(A) Antibacterial effects of AgNCs/RB on oral bacteria after 24-h incubation (n=5, mean ± SD). Turbidities of *S. mutans*, *P. gingivalis*, and *A. actinomycetemcomitans*: *,

P<0.05 vs. 0 μg/mL AgNCs/RB; †, *P*<0.05 vs. 0.01 μg/mL AgNCs/RB; #, *P*<0.05 vs. 0.1 μg/mL AgNCs/RB; and $, *P*<0.05 vs. 1 μg/mL AgNCs/RB. (B) SEM and TEM observation and LIVE/DEAD BacLight staining of *S. mutans* after 24-h incubation in control (no application of AgNCs/RB) and AgNCs/RB groups. Scale bar represents 50 μm (SEM and LIVE/DEAD staining) and 500 nm (TEM). AgNCs, silver nanoclusters; au, arbitrary unit; LED, light-emitting diode; RB, rose bengal; SD, standard deviation; SEM, scanning electron microscopy; TEM, transmission electron microscope.

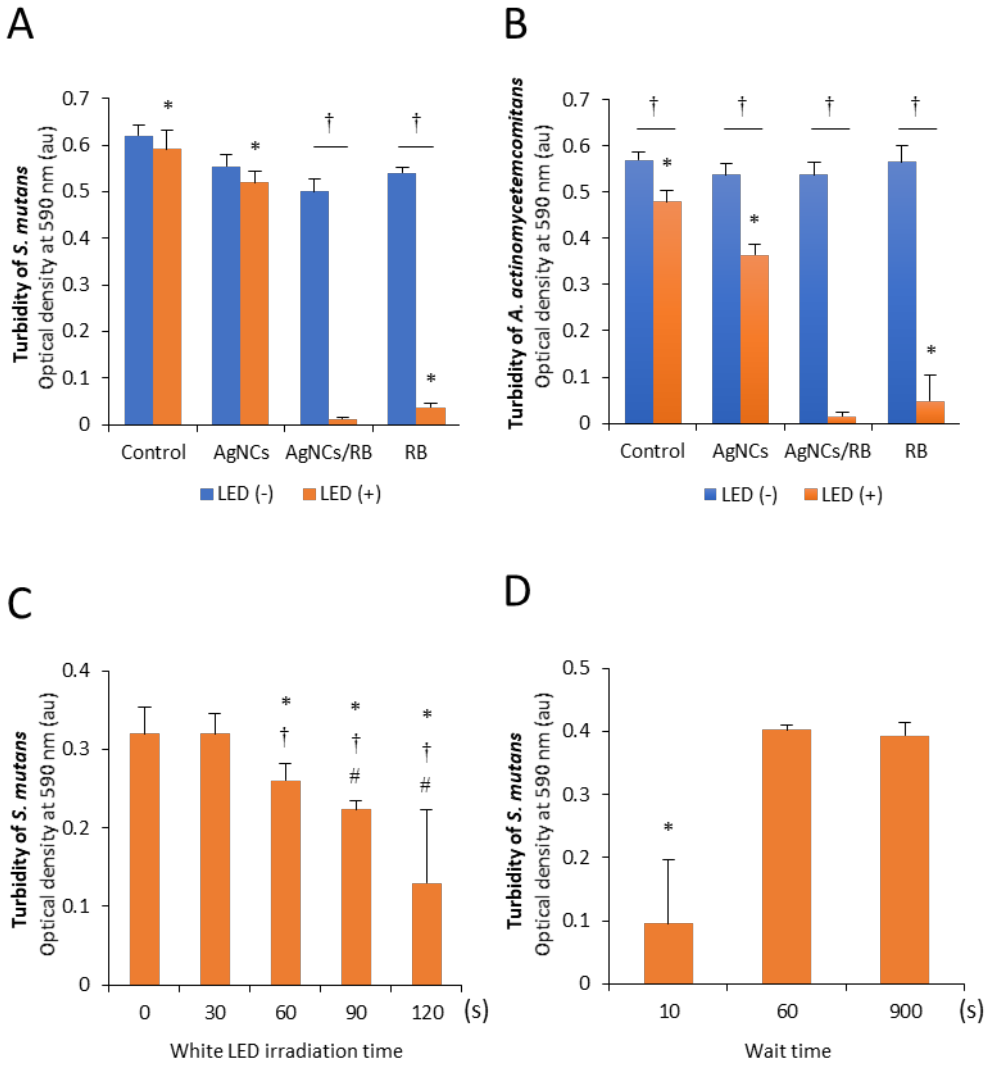

Fig. 3. Antibacterial characterization of AgNCs/RB

(A, B) Turbidities of control (no application), AgNCs, RB, and AgNCs/RB groups of *S. mutans* (n=5, mean ± SD) (A) and *A. actinomycetemcomitans* (n=4, mean ± SD) (B). *, $P<0.05$ vs. AgNCs/RB with LED (+); †, $P<0.05$. (C) Turbidity of *S. mutans* with increasing white LED irradiation time (0, 30, 60, 90, and 120 s) (n=5, mean ± SD). *, $P<0.05$ vs. 0 s; †, $P<0.05$ vs. LED irradiated for 30 s; and #, $P<0.05$ vs. LED irradiated for 60 s. (D) Turbidity of *S. mutans* in AgNCs/RB-containing medium. *S. mutans* suspension was mixed into the medium 10, 60, and 900 s after LED irradiation (n=5,

mean ± SD). *, $P<0.05$ vs. 60 and 900 s. AgNCs, silver nanoclusters; au, arbitrary unit; LED, light-emitting diode; RB, rose bengal; SD, standard deviation.

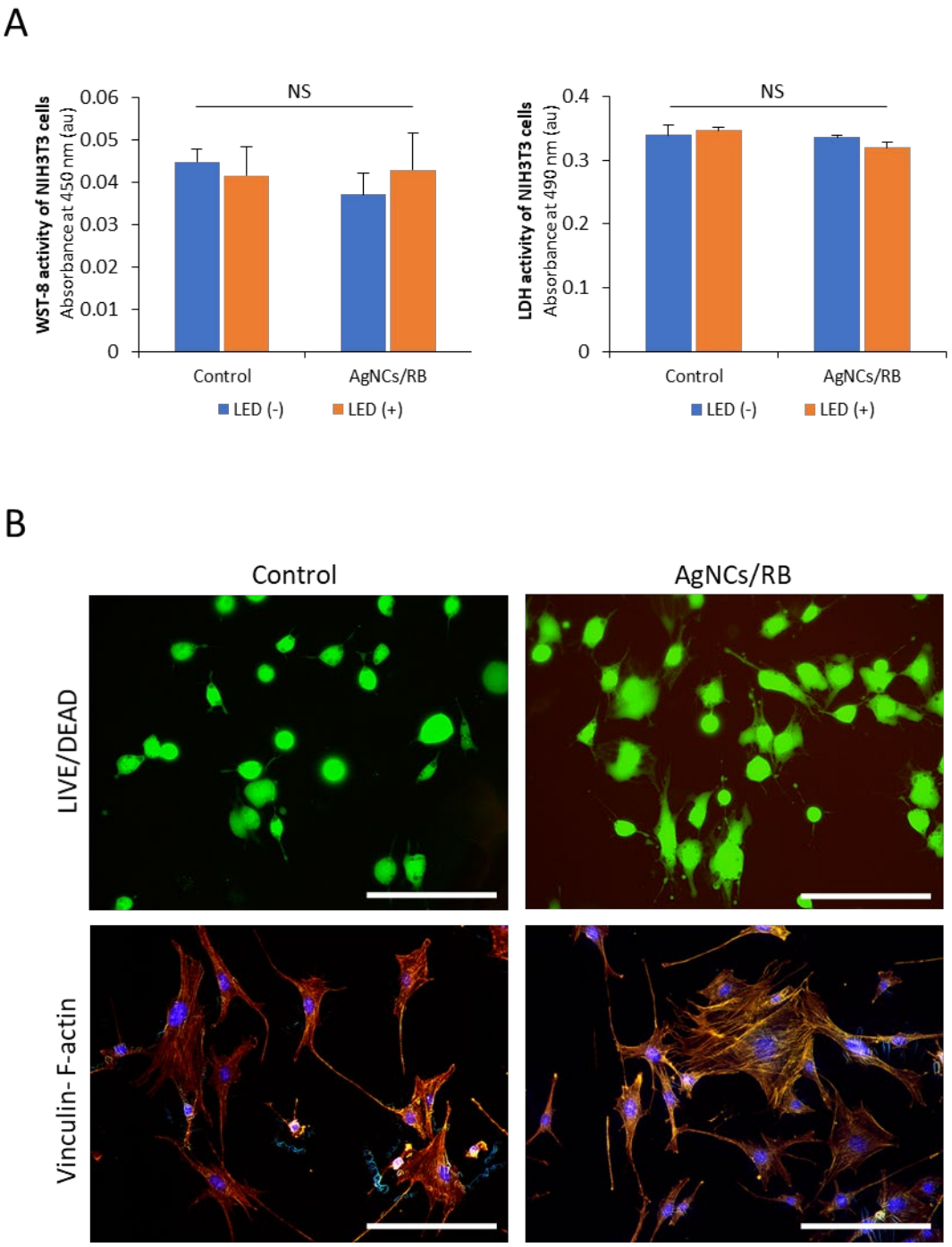

Fig. 4. Assessments of cytotoxic effects of AgNCs/RB

(A) WST-8 and LDH activities of NIH3T3 cells in control (no application) and AgNCs/RB groups (n=6, mean ± SD). (B) LIVE/DEAD BacLight staining and vinculin/F-actin double staining of NIH3T3 cells after 24-h incubation in control and AgNCs/RB groups. Scale bar represents 50 μm. AgNCs, silver nanoclusters; au,

arbitrary unit; LDH, lactate dehydrogenase; LED, light-emitting diode; NS, not significant; RB, rose bengal; SD, standard deviation; WST, water-soluble tetrazolium salt.